Bone Reports 10 (2019) 100197

Contents lists available at ScienceDirect

Bone Reports

journal homepage: www.elsevier.com/locate/bonr

Insulin Receptor deletion in S100a4-lineage cells accelerates age-related bone loss

Valentina Studentsova, Emma Knapp, Alayna E. Loiselle*

Center for Musculoskeletal Research, University of Rochester Medical Center, Rochester, NY 14642, United States of America

ARTICLE INFO

Keywords:
Insulin receptor
S100a4
Bone
Bone homeostasis
Aging

ABSTRACT

Type I and Type II Diabetes dramatically impair skeletal health. Altered Insulin Receptor (IR) signaling is a common feature of both diseases, and insulin has potent bone anabolic functions. Several previous studies have demonstrated that loss of IR in bone cells results in disrupted bone homeostasis during early post-natal growth. Here we have deleted IR in S100a4-lineage cells ($IRcKO^{S100a4}$) and assessed the effects on bone homeostasis in both young (15 weeks) and older adult (48 weeks) mice. S100a4-Cre has previously been shown to target the perichondrium during bone development, and here we show that S100a4 is expressed by adult trabecular and cortical bone cells, and that S100a4-Cre effectively targets adult bone, resulting in efficient deletion of IRβ. Deletion of IRβ in S100a4-lineage cells does not affect initial bone acquisition or homeostasis with no changes in cortical, trabecular or mechanical properties at 15-weeks of age, relative to wild type (WT) littermates. However, by 48-weeks of age, $IRcKO^{S100a4}$ mice display substantial declines in trabecular bone volume, bone volume fraction and torsional rigidity, relative to age-matched WT controls. This work establishes the utility of using S100a4-cre to target bone and demonstrates that IRβ in S100a4-lineage cells is required for maintenance of bone homeostasis in adult mice.

1. Introduction

Both Type I and Type II Diabetes dramatically impair skeletal health. Type I Diabetes both accelerates the onset and increases the risk of osteopenia and osteoporosis (Khan and Fraser, 2015; Gunczler et al., 1998; Hadjidakis et al., 2006), while Type II Diabetes can actually increase bone mineral density (van Daele et al., 1995; Rakic et al., 2006). However, in both cases, bone homeostasis is disrupted, including decreased bone quality (reviewed in (Saito and Marumo, 2013)), resulting in a substantial increase in fracture risk (Vestergaard, 2007; Janghorbani et al., 2006). Moreover, in both clinical and pre-clinical models impaired healing following bone fracture is observed in Type I and Type II Diabetics (Thrailkill et al., 2005; Brown et al., 2014; Kayal et al., 2007; Jiao et al., 2015). Despite their different pathophysiologies, disruptions in Insulin Receptor (IR) function occur in both disease states due to a decrease in insulin production in Type I Diabetes, and a decrease in insulin sensitivity with type II Diabetes. This conservation of altered Insulin Receptor signaling suggests an important role for IR in diabetic pathologies, including disrupted bone homeostasis. Insulin is a potent regulator of osteoblast function, with insulin stimulating collagen synthesis (Rosen and Luben, 1983), and production of alkaline phosphatase (Kream et al., 1985). Importantly, exogenous insulin can also reverse deficits in bone formation during healing in diabetic mice (Thrailkill et al., 2005). Several in vivo studies have examined the effects of IR conditional deletion in osteoblast-lineage cells (Ferron et al., 2010; Fulzele et al., 2010; Thrailkill et al., 2014), and demonstrate that IR deletion in osteoblasts impairs bone growth and homeostasis during skeletal maturation. However, the long-term effects of IR loss of function have not been studied, although there is high clinical relevance to this approach as increasing fracture risk is associated with increasing duration of Diabetes (Nicodemus et al., 2001).

While the effects of IR deletion during different stages of osteoblast maturation are well understood, the effects of IR deletion in other bone-associated cells are unknown. S100a4 belongs to the S100 family of EF-hand Ca^{2+}-binding proteins, which are expressed in highly cell- and tissue-specific patterns (Leclerc et al., 2009). We have recently demonstrated the effects of IR deletion in S100a4-lineage cells on tendon homeostasis (Studentsova et al., 2018) in order to better understand the mechanisms underlying diabetic tendinopathy. However, given that S100a4 is a potent negative regulator of osteoblast differentiation in vitro (Duarte et al., 2003), with these effects mediated in part through inhibition of mineralization (Kim et al., 2017), and the importance of IR in maintaining skeletal homeostasis, we also examined the bone phenotype in these mice. $S100a4^{-/-}$ mice have larger bones, with

* Corresponding author at: Center for Musculoskeletal Research, 601 Elmwood Ave. Box 665, Rochester, NY 14642, United States of America.
E-mail address: Alayna_loiselle@urmc.rochester.edu (A.E. Loiselle).

https://doi.org/10.1016/j.bonr.2019.100197
Received 4 October 2018; Received in revised form 28 January 2019; Accepted 1 February 2019
Available online 05 February 2019

increased bone density, and decreased osteoclastogenesis, while ShRNA knock-down of S100a4 increases cortical thickness (Erlandsson et al., 2013). S100a4 is expressed in perichondrium cells during bone development (Inubushi et al., 2018), and Duarte et al. demonstrated that S100a4 is expressed by pre-osteoblasts, followed by a decline in expression in terminally differentiated osteocytes, in vitro (Duarte et al., 2003). However, the expression pattern of S100a4 in adult bone is not clear. Here, we demonstrate that S100a4-lineage cells are found in cortical and trabecular bone, as well as the bone marrow. We generated S100a4-lineage specific IR conditional knockout mice and tested the hypothesis that conditional deletion of IRβ in *S100a4*-lineage cells would disrupt bone homeostasis leading to decreased mechanical properties. Loss of IR signaling in S100a4-lineage cells resulted in accelerated bone loss during aging and a significant reduction in torsional rigidity at 48-weeks of age, relative to WT littermates.

2. Materials and methods

2.1. Ethics statement

All animal studies were approved and conducted in accordance with the University of Rochester University Committee on Animal Resources (UCAR) and the National Institutes of Health guide for the care and use of Laboratory animals.

2.2. Animals

S100a4-Cre (#12641), $IR^{flox/flox}$ (#6955) (Bruning et al., 1998), Rosa-Ai9 (#7909) (Madisen et al., 2010), S100a4-$GFP^{Promoter}$ (#12893) (Iwano et al., 2002) mice were purchased from Jackson Laboratories (Bar Harbor, ME).

2.3. Metabolic data

As part of a study focusing on the tendon, changes in weight, fasting blood glucose, glucose tolerance and body fat percentage were assessed between WT and $IRcKO^{S100a4}$ mice at 48 weeks of age (Studentsova et al., 2018). Fasting blood glucose was measured following a five-hour fast, using a OneTouch2 blood glucometer (LifeScan Inc. Milpitas, CA). Glucose tolerance was then measured at 15, 30, 60, and 120 min following administration of a 10 μL/g bolus of 20% glucose in PBS via intraperitoneal injection. Body fat percentage was measured using the PIXImus dual-energy X-ray absorptiometer (DXA) (GE Lunar PIXImus, GE Healthcare, WI).

2.4. Spatial localization and characterization of $S100a4^+$ cells

To assess the spatial localization of S100a4-lineage cells and cells actively expressing S100a4, S100a4-Cre; Rosa-$Ai9^{F/+}$ ($S100a4^{Ai9}$) and S100a4-$GFP^{Promoter}$ mice were used, respectively. Male mice were sacrificed at 15- and 48-weeks of age and femurs were harvested and processed for cryosectioning. Briefly, femurs were fixed in 10% neutral buffered formalin (NBF) for 24 h, partially decalcified for 3 days in 14% Callis EDTA (Callis and Sterchi, 1998), immersed in 30% sucrose in PBS overnight and embedded in Cryomatrix. Serial 8 μm sections were cut through the sagittal-plane of the femur and placed on Cryotape (Section-Lab, Japan). Sections were then stained with Hoechst 33342 (#R37605, ThermoFisher), cover slipped (Prolong Gold #P36930, ThermoFisher, Waltham, MA), and digitally imaged using an Olympus slide scanner for endogenous Ai9 (TdTomato) and GFP fluorescence. The proportion of S100a4-lineage ($S100a4^{Ai9+}$) and S100a4-$GFP^{promoter}$ ($S100a4^{GFP+}$) cells were quantified in cortical and trabecular bone (n = 3 slides per specimen, 4 specimens per group) as a proportion of total $DAPI^+$ nuclei. Cortical bone was quantified in an area 450 μm long × 150 μm wide, and trabecular bone was quantified in a 500 μm^2 area. To determine the potential fate of S100a4-lineage cells in bone, co-immunofluorescence for $S100a4^{Ai9}$ (Red Fluorescent protein) and Osterix (pre-osteoblasts) or Osteocalcin (mature osteoblasts) was conducted. Briefly, sections were blocked with Normal Donkey Serum (#017-000-121, Jackson ImmunoResearch) and F(ab) fragment Goat Anti-mouse IgG (1:1000, #Ab6668, Abcam), then incubated with the following primary and secondary antibodies: Rabbit-anti-RFP (1:500, #Ab62341, Abcam) with a Donkey-anti-Rabbit TRITC secondary antibody (1:100, # 711-296-152, Jackson ImmunoResearch); Mouse-anti-Osteocalcin (1:50, #sc0365797, Santa Cruz) with a Donkey-anti-mouse FITC secondary (1:100, # 715-096-150, Jackson ImmunoResearch); Rabbit-anti-Osterix (1:250, #Ab209484, Abcam) with a Donkey-anti-Rabbit FITC secondary (1:100, # 711-096-152, Jackson ImmunoResearch). Fluorescent imaging was conducted using a VS120 Virtual Slide Microscope (Olympus, Waltham, MA).

2.5. Protein isolation and western blotting

Following sacrifice, femurs were harvested, stripped of surrounding soft tissue and the marrow was flushed. Total protein was harvested from the metaphysis via homogenization in RIPA buffer containing protease/phosphatase inhibitors (#78445, ThermoFisher). Western Blots were probed with the following antibodies: Insulin Receptor β (1:100, #SC-20739, Santa Cruz), βactin (1:2500, #A2228, Sigma), Goat anti-rabbit secondary (1:2000, #1706515, BioRad). Blots were then imaged using West Pico (#34578) or Femto substrate (#34095, ThermoFisher). Western blots are representative of three independent experiments.

2.6. RNA isolation and qPCR

Femurs (n = 2 per genotype) were harvested, stripped of surrounding soft tissue and the marrow was flushed. Femurs were then homogenized in TRIzol Reagent (ThermoFisher Scientific), and total mRNA was extracted. A total of 500 ng of mRNA was reverse transcribed in to cDNA using qScript cDNA Synthesis Kit (#95047-500, QuantaBio), followed by qPCR analysis of Insulin Receptor β expression. IRβ expression was normalized to β-actin.

2.7. Micro CT analysis

Following sacrifice, the femur was isolated and cleaned of excess soft tissue. Femurs were imaged using VivaCT 40 cone-beam CT (Scanco Medical) with an X-ray potential of 55,000 V, and surrounding air was used as the scanning medium to ensure proper alignment and immobilization. Images were reconstructed in 3D at a resolution of 10 μM (n = 5–8 per genotype per age). Cortical bone was analyzed from the distal end of the third trochanter, where the lateral projection changes from a sharp point to a rounded point. This initial slice and the next 30 distal slices were included in the region of interest. Contours were drawn at the bone surface to exclude any soft tissue outside the bone. The threshold was set at 340, equivalent to a linear attenuation coefficient of 2.720 cm^{-1}. Analysis of femur trabecular bone occurred from the proximal end of the growth plate proximally for 100 slices (10.5-micron slices). Contours were close-drawn to the cortical shell, and then shrunk to 95% in X and Y dimensions to avoid any inclusion of cortical bone. A threshold of 280 was used, which is equivalent to a linear attenuation coefficient of 2.240 cm^{-1}.

2.8. Biomechanical torsion testing

Following micro CT, the ends of the femurs were cemented (Bosworth Company) in aluminum tube holders and tested using an EnduraTec TestBench™ system (Bose Corporation, Eden Prairie, MN). The femurs were tested in torsion until failure at a rate of 1 deg/sec.

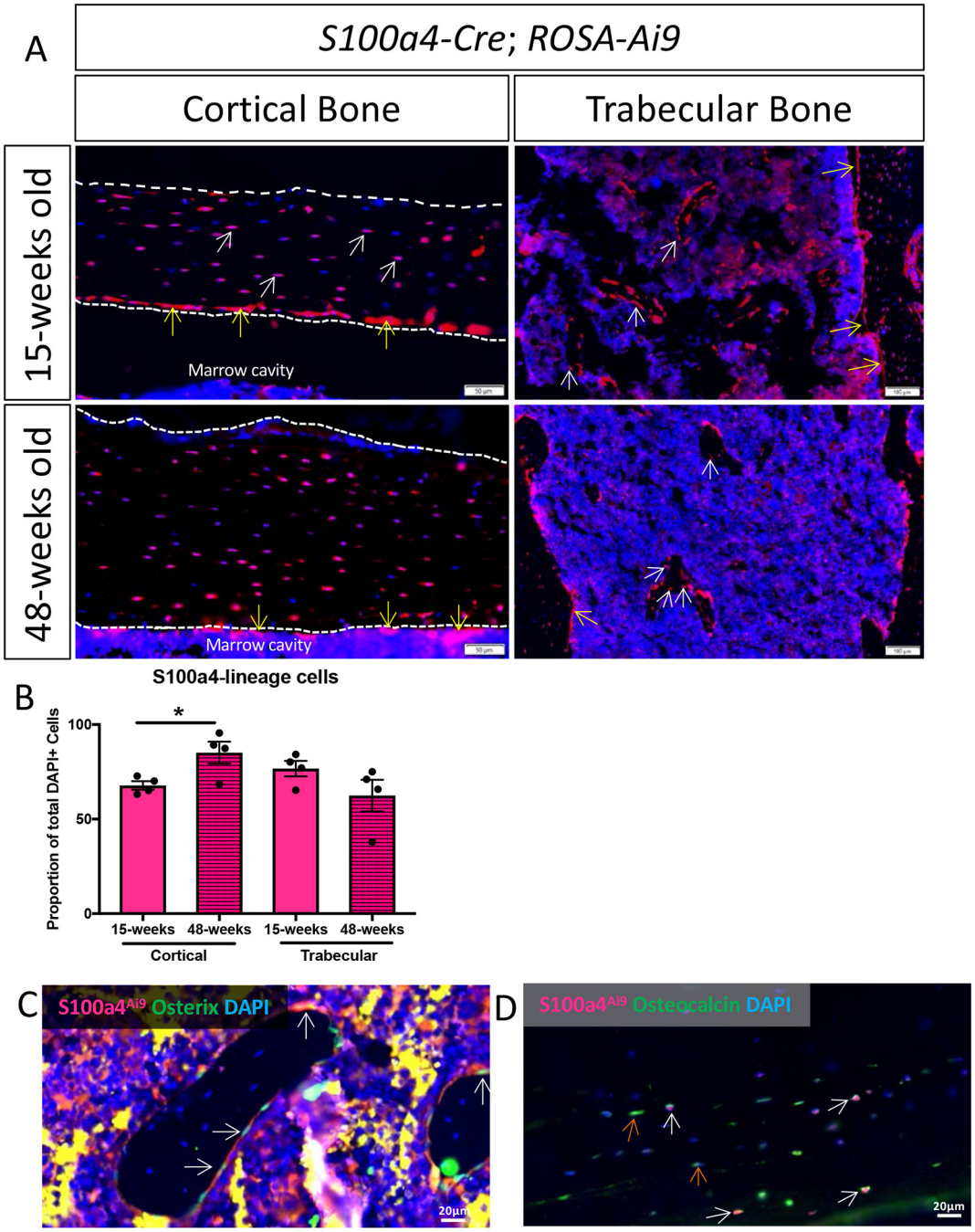

Fig. 1. S100a4-lineage cells are located in cortical and trabecular bone. (A) To determine the spatial localization of S1004-lineage cells in 15- and 48-week old femurs S100a4-Cre; Rosa-Ai9 (S100a4^{Ai9}) mice were used. At 15- and 48-weeks of age S100a4-lineage cells were located in the cortical and trabecular bone, and the bone marrow. Scale bars represent either 50 or 100 μm as noted on each image. White arrows indicate trabecular osteoblasts that are S100a4^{Ai9+}. Yellow arrows identify S100a4^{Ai9+} cells lining the endosteum. (B) To determine the proportion of S100a4^{Ai9+} cells in cortical and trabecular bone, S100a4^{Ai9+} cells/DAPI^{+} cells were quantified in each compartment. (*) indicates $p < 0.05$ between 15- and 48-week old animals. (C & D) Co-immunofluorescence for Red Fluorescent Protein (S100a4^{Ai9+}) and (C) Osterix (green) or (D) Osteocalcin (green). White arrows indicate co-expression of S100a4^{Ai9} and Osterix or Osteocalcin. Orange arrows in (D) identify Osteocalcin^{+} cells that are not derived from the S100a4-lineage. Sections were also stained with DAPI to identify nuclei. Scale bars represent 20 μm. (For interpretation of the references to color in this figure, the reader is referred to the web version of this article.)

2.9. Statistical analyses

Data are presented ± Standard Error of the Mean (SEM). For micro CT and torsion testing, statistically significant differences were determined using two-way ANOVA with Tukey post-test. Differences in quantification of S100a4^{Ai9+} and S100a4^{GFP+} cells, and qPCR were determined by unpaired *t*-test. Differences were considered statistically significant at $p < 0.05$.

3. Results

3.1. S100a4-lineage cells are found in trabecular bone osteoblasts and cortical bone osteocytes

To trace S100a4-lineage cells in bone, femurs were harvested at 15 and 48 weeks of age from male S100a4-Cre; Rosa-Ai9 mice, resulting in Ai9 (TdTomato) fluorescence in cells that have undergone Cre-

mediated recombination driven by the S100a4 promoter. By 15 weeks of age, S100a4-lineage cells had become cortical osteocytes and trabecular lining osteoblasts (white arrows, Fig. 1A), and S100a4-lineage cells were also observed lining the endosteal surface (yellow arrows, Fig. 1A), and in the bone marrow (Fig. 1A). Consistent with this, S100a4-lineage cells remained in the cortical bone, and trabecular lining cells at 48 weeks of age (Fig. 1A). To assess potential changes in S100a4-lineage cell localization and abundance over time, $S100a4^{Ai9+}$ cells were quantified in cortical and trabecular bone at 15- and 48-weeks of age. A significant increase in $S100a4^{Ai9+}$ cells was observed in cortical bone from 15 to 48 weeks (+25%), with 67% (± 2.22) of cortical bone cells being $S100a4^{Ai9+}$ at 15-weeks, and 85% (± 5.85) $S100a4^{Ai9+}$at 48-weeks ($p = 0.03$). No change in the proportion of $S100a4^{Ai9+}$ cells was observed in trabecular bone between 15-weeks (76% ± 4.07 $S100a4^{Ai9+}$) and 48-weeks (62% ± 8.40 $S100a4^{Ai9+}$) ($p = 0.17$) (Fig. 1B).

To determine the fate of S100a4-lineage cells, co-immunofluorescence for Ai9 (red fluorescent protein) and Osterix (pre-osteoblasts) and Osteocalcin (mature osteoblasts) was conducted. Many cells that expressed both $S100a4^{Ai9}$ and Osterix were observed lining trabecular bone (white arrows, Fig. 1C). In addition, co-localization of $S100a4^{Ai9}$ and Osteocalcin was observed in cortical bone (white arrows, Fig. 1D). However, there were also $Osteocalcin^{+}$ cells that lacked $S100a4^{Ai9}$ expression (orange arrows, Fig. 1D), suggesting they were not derived from S100a4-lineage cells.

To determine which cells actively express S100a4 at a given time, $S100a4GFP^{Promoter}$ mice were used. At 15 weeks, a few $S100a4GFP^{Promoter}$ cells were observed in the bone marrow, and periosteum, however, very few $S100a4GFP^{Promoter}$ cells were observed in cortical bone. In addition, $S100a4GFP^{Promoter}$ cells were observed in trabecular bone (Fig. 2A). By 48 weeks more cortical osteocytes actively expressed S100a4, and $S100a4^{GFP+}$ cells remained in trabecular bone (Fig. 2A). Quantitatively, a significant increase in the proportion of $S100a4GFP^{promoter+}$ cells were observed in cortical bone of 48-week old mice, relative to 15-weeks (15-weeks: 16.4% ± 1.17; 48-weeks: 40.4% ± 2.69, $p = 0.0002$) (Fig. 2B). No change in the proportion of $S100a4GFP^{promoter+}$ cells was observed between 15- and 48-week old animals (15-weeks: 49.7% ± 2.63; 48-weeks: 47.5% ± 1.92, $p = 0.5$) (Fig. 2B).

3.2. $IRcKO^{S100a4}$ decreases IR expression in bone

No changes in body weight, or fasting blood glucose were observed between groups (Studentsova et al., 2018) at 48 weeks of age, indicating that $IRcKO^{S100a4}$ allows the delineation of IR function in S100a4-lineage cells independent of systemic metabolic changes. To confirm that $IRcKO^{S100a4}$ effectively reduces IR expression in the bone, total mRNA and protein was isolated from the metaphysis of WT and $IRcKO^{S100a4}$ bones from 48-week-old animals. A significant 63% reduction in IRβ mRNA was observed in $IRcKO^{S100a4}$ femurs, relative to WT at 48-weeks of age ($p = 0.0013$) (Fig. 3A). Consistent with this, a substantial reduction in IRβ protein was observed in $IRcKO^{S100a4}$ bones, relative to WT (Fig. 3B), indicating efficient knock-down of IRβ in bone using S100a4-Cre.

3.3. $IRcKO^{S100a4}$ enhances age-related trabecular bone loss

At 15 and 48 weeks of age no significant changes in Cortical Bone Volume (Ct. BV), Cortical Bone Volume/Total Volume (Ct. BV/TV), or Cortical Thickness (Ct. Th) were observed between WT and $IRcKO^{S100a4}$ femurs (Fig. 4A–E). Cortical Mineral Density was significantly increased from 15 to 48 weeks in both WT and $IRcKO^{S100a4}$, however, no differences between genotypes were observed at either age (Fig. 4F). Trabecular BV was not different between WT and $IRcKO^{S100a4}$ at 15 weeks of age ($p = 0.73$). At 48 weeks Tb. BV was decreased in both WT and $IRcKO^{S100a4}$ relative to their respective genotypes at 15 weeks, indicative of age-related bone loss. In addition, Tb.BV was significantly decreased in $IRcKO^{S100a4}$ femurs relative to WT at 48 weeks (WT: 0.188 mm3 ± 0.017; $IRcKO^{S100a4}$: 0.048 ± 0.009, $p = 0.002$) (Fig. 5A & B). Consistent with this, Tb. BV/TV was decreased in both genotypes at 48 weeks, relative to their respective genotypes at 15-weeks ($p < 0.0001$). In addition, Tb. BV/TV was significantly decreased in $IRcKO^{S100a4}$ at 48 weeks, relative to age-matched WT femurs (WT: 0.073 ± 0.007; $IRcKO^{S100a4}$: 0.026 ± 0.0023, $p = 0.0024$) (Fig. 5C). While Tb. N (WT: 9% decrease, $p < 0.0001$; $IRcKO^{S100a4}$: 12% decrease, $p < 0.0001$), and Tb.Sp (WT: +99%, $p = 0.0018$, $IRcKO^{S100a4}$: +141%, $p < 0.0001$) were significantly altered as a function of age in both WT and $IRcKO^{S100a4}$ animals, no differences were observed between genotypes at either time-point for any of these parameters (Fig. 5D & E). No differences in Trabecular Thickness were observed as a function of age or genotype (Fig. 5F).

3.4. $IRcKO^{S100a4}$ decreases torsional rigidity in aged mice

No changes in ultimate torque were observed between WT and $IRcKO^{S100a4}$ femurs at 15 or 48-weeks age (Fig. 6A). In addition, no differences in Torsional Rigidity (T.R.) were observed between WT and $IRcKO^{S100a4}$ femurs at 15 weeks of age (Fig. 6B). T.R. was not significantly different between 15 and 48-week old WT mice ($p = 0.91$). However, a significant reduction in T.R. was observed in 48-week-old $IRcKO^{S100a4}$ femurs, relative to both 48-week old WT (26% decrease, $p = 0.02$) and 15-week old $IRcKO^{S100a4}$ (33% decrease, $p = 0.008$).

4. Discussion

Type I and Type II Diabetes dramatically impair bone health, leading to a substantial increase in fracture risk (Janghorbani et al., 2006; Chau et al., 2003). Previous work has demonstrated that bone is an insulin target tissue, with osteoblasts expressing functional insulin receptors, and insulin exerting bone anabolic effects (Rosen and Luben, 1983). Several studies have assessed the effects of IR deletion in distinct bone cell populations and demonstrate disruptions in bone homeostasis (Ferron et al., 2010; Fulzele et al., 2010; Thrailkill et al., 2014). In the present study we have used the S100a4-Cre driver and demonstrate effective targeting of bone, and efficient deletion of IRβ in $IRcKO^{S100a4}$. Loss of IRβ in S100a4-lineage cells results in bones that are more susceptible to age-related declines in trabecular bone, and decreased torsional rigidity, relative to age-matched WT mice.

While models of Type I and Type II Diabetes clearly demonstrate the impact of systemic alterations in IR signaling on bone, a series of elegant studies have defined the effects of IR deletion specifically in bone cells. Fulzele et al. demonstrated the IR was expressed in trabecular bone osteoblasts, and that IR deletion using Osteocalcin-Cre (Oc-Cre) resulted in impaired bone acquisition. Deficits in trabecular bone were especially pronounced at 3 and 6-weeks of age, while minimal differences were observed between genotypes at 12-weeks of age (Fulzele et al., 2010). Deletion of IR using Col1a1-Cre also disrupted initial bone formation with decreases in bone volume fraction and bone formation rate observed at 8 weeks of age, relative to WT (Ferron et al., 2010). Finally, Thrailkill et al. utilized Osterix-Cre (Osx-Cre) to drive IR deletion in osteoprogenitors, which resulted in decreased trabecular bone volume and thickness at 12-weeks of age (Thrailkill et al., 2014). Interestingly, we did not observe any alterations in initial bone acquisition (15-weeks of age) in $IRcKO^{S100a4}$ mice, while dramatic impairments in trabecular bone maintenance were observed at 48-weeks of age. However, bone phenotypes were not assessed past 12-weeks of age in previous studies, so it is unknown how loss of IR in these populations may alter bone homeostasis during aging. Interestingly, the dramatic reduction in torsional rigidity observed in 48-week old $IRcKO^{S100a4}$ femurs is not accompanied by a concomitant decrease in cortical bone parameters. While the reason for this discrepancy is unknown, it is possible that there is a reduction in cortical bone quality in $IRcKO^{S100a4}$

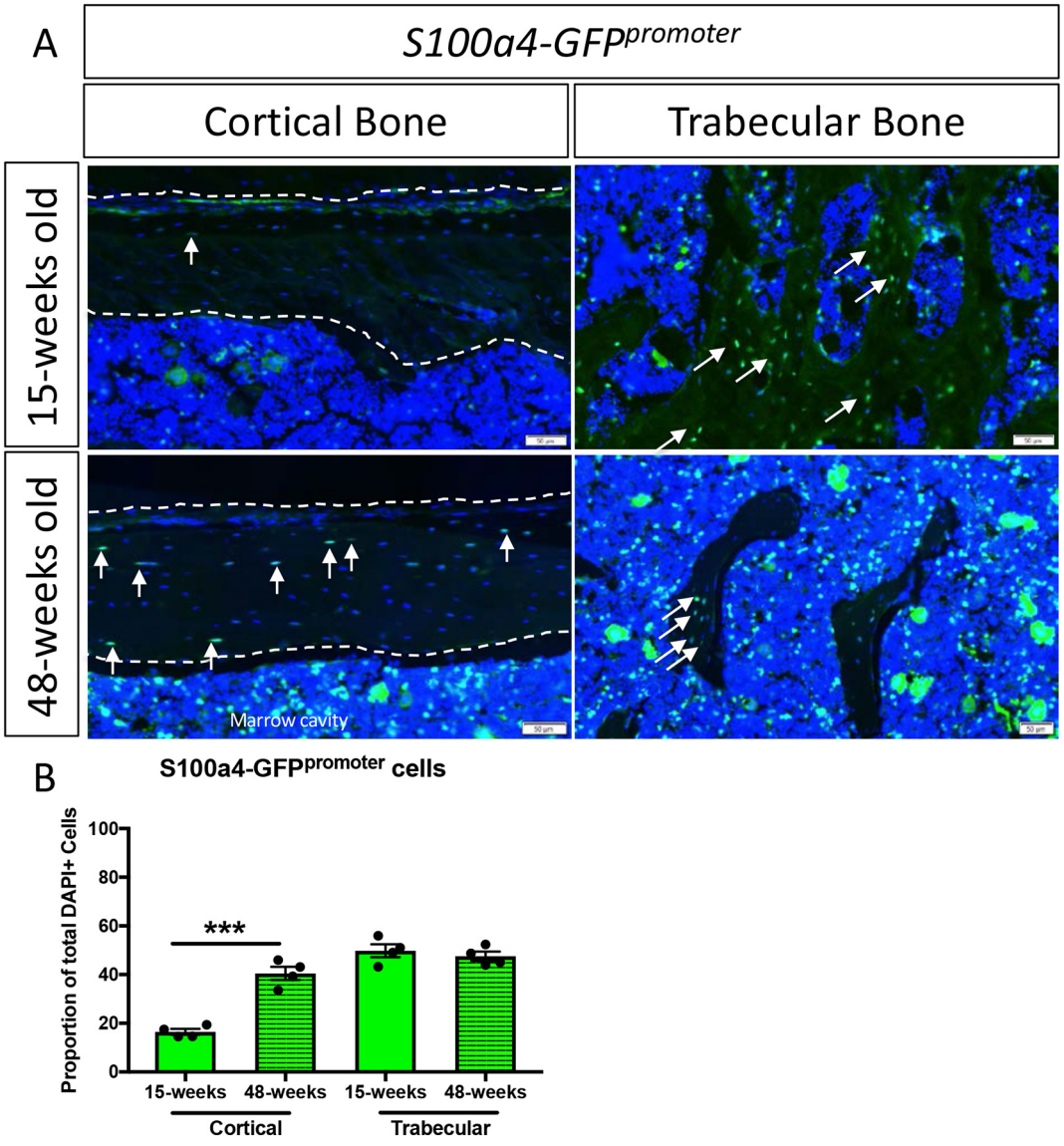

Fig. 2. Cells actively expressing S100a4 are located in the trabecular bone, and cortical bone of aged 48-week but not 15-week old mice. To determine the spatial localization of cells actively expressing S100a4 at 15 and 48-weeks of age S100a4GFP^{promoter} were used. At 15 weeks of age several S100a4^{+} cells were located in trabecular bone and the bone marrow, with very few S100a4^{GFP+} cells in the cortical bone. At 48-weeks S100a4^{+} cells were observed in cortical and trabecular bone, as well as the bone marrow. Scale bars represent 50 μm. White arrows indicate S100a4^{GFP+} cells. (B) S100a4^{GFP+} cells were quantified in cortical and trabecular bone at 15- and 48-weeks of age. S100a4^{GFP+} cells were significantly increased in cortical bone at 48-weeks, relative to 15-weeks. No change in the proportion of S100a4^{GFP+} cells was observed in trabecular bone between 15 and 48 weeks of age. (***) indicates p = 0.0002.

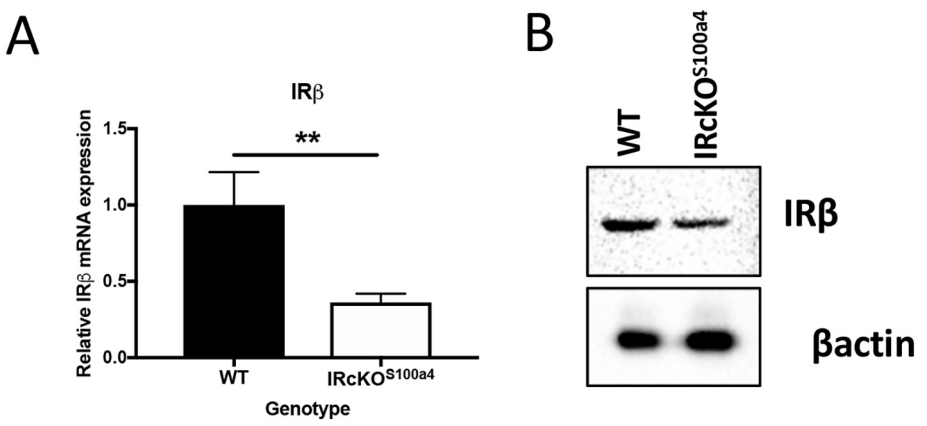

Fig. 3. Deletion of IR in S100a4-lineage cells decreases IR expression in bone. At 48 weeks of age total mRNA and protein was isolated from the femurs of WT and IRcKO^{S100a4} mice. (A) qPCR analysis demonstrates a significant 64% reduction in IRβ mRNA expression in IRcKO^{S100a4} relative to WT. (B) Western blotting for IRβ demonstrates a substantial decrease in IRβ protein expression in IRcKO^{S100a4} relative to WT. Expression was normalized to βactin.

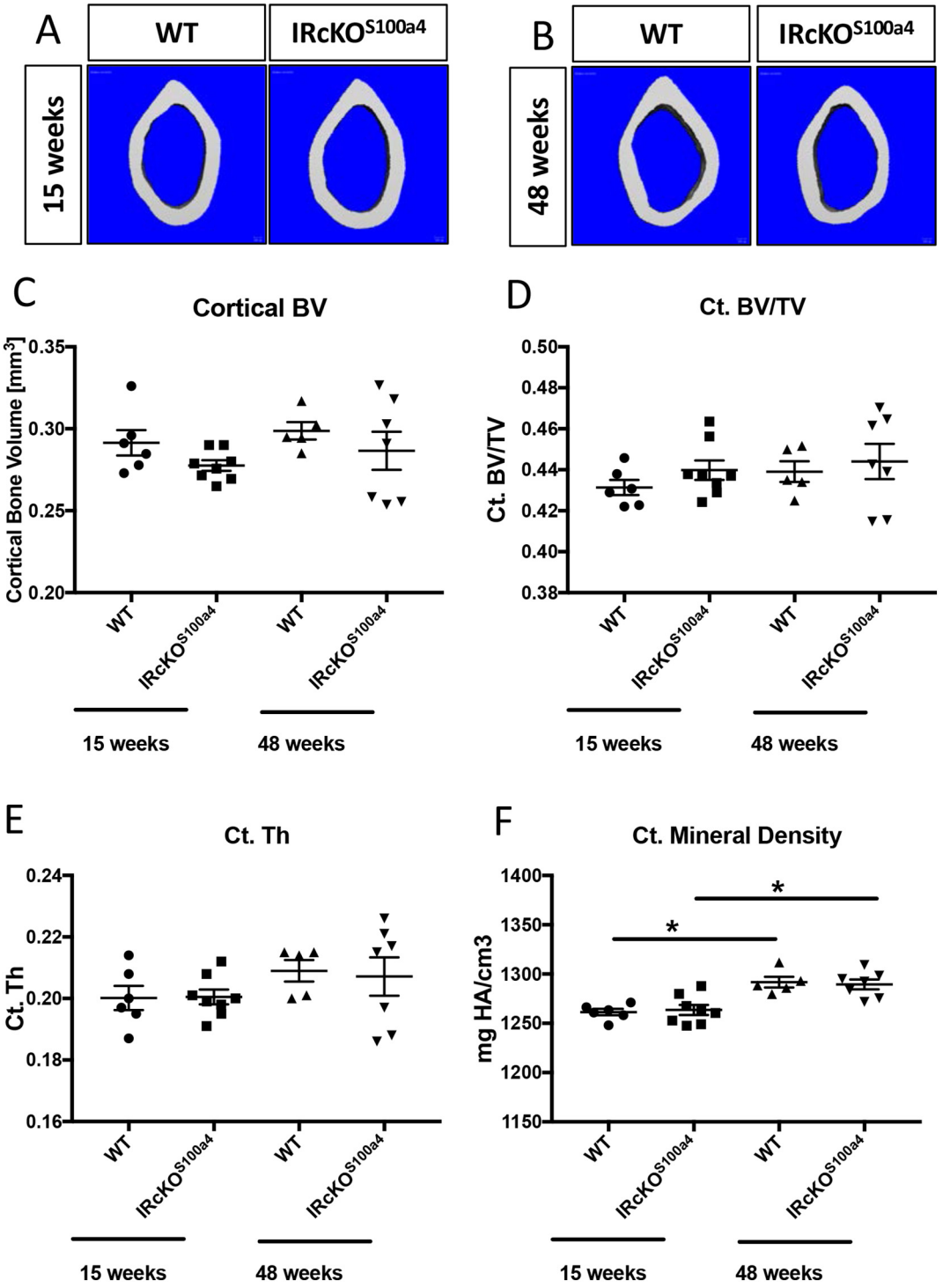

Fig. 4. IRcKO^{S100a4} does not alter cortical bone parameters during aging. (A & B) 3D micro CT reconstructions of the cortical bone of the femurs from (A) 15-week old, and (B) 48-week-old male mice. (C–F) Micro CT analysis of (C) Cortical Bone Volume, (D) Cortical Bone Volume/Total Volume, (E) Cortical Thickness, and (F) Cortical Mineral Density from WT and IRcKO^{S100a4} femurs at 15 and 48 weeks of age. (*) indicates $p < 0.05$.

femurs. While we have not assessed this possibility, future studies using a technique such as reference point indentation (Randall et al., 2009) may help clarify this possibility, as RPI is strongly associated with bone mechanical properties (Gallant et al., 2013). Importantly, deletion of IR using both Col1a1-Cre and OC-Cre resulted in altered systemic metabolism, including increased adiposity and body weight (Fulzele et al., 2010), and altered glucose tolerance (Ferron et al., 2010; Fulzele et al., 2010). In contrast, IR deletion in S100a4-lineage cells does not alter metabolism or induce obesity, even up to 48-weeks of age. Thus, IRcKO^{S100a4} permits assessment of IR function in this cell population without the confounding effects of altered systemic metabolism.

The difference in age-related bone phenotypes between IR deletion in osteoblast-lineage cells and S100a4-lineage cells may suggest a potential shift in the cell population(s) that rely on IR to maintain bone homeostasis over the course of aging, with a greater reliance of S100a4-lineage cells with increasing age. Here we show that the proportion of S100a4^{GFP+} cortical bone cells is markedly reduced relative to S100a4^{Ai9+} cortical bone cells at both 15- and 48-weeks. Therefore,

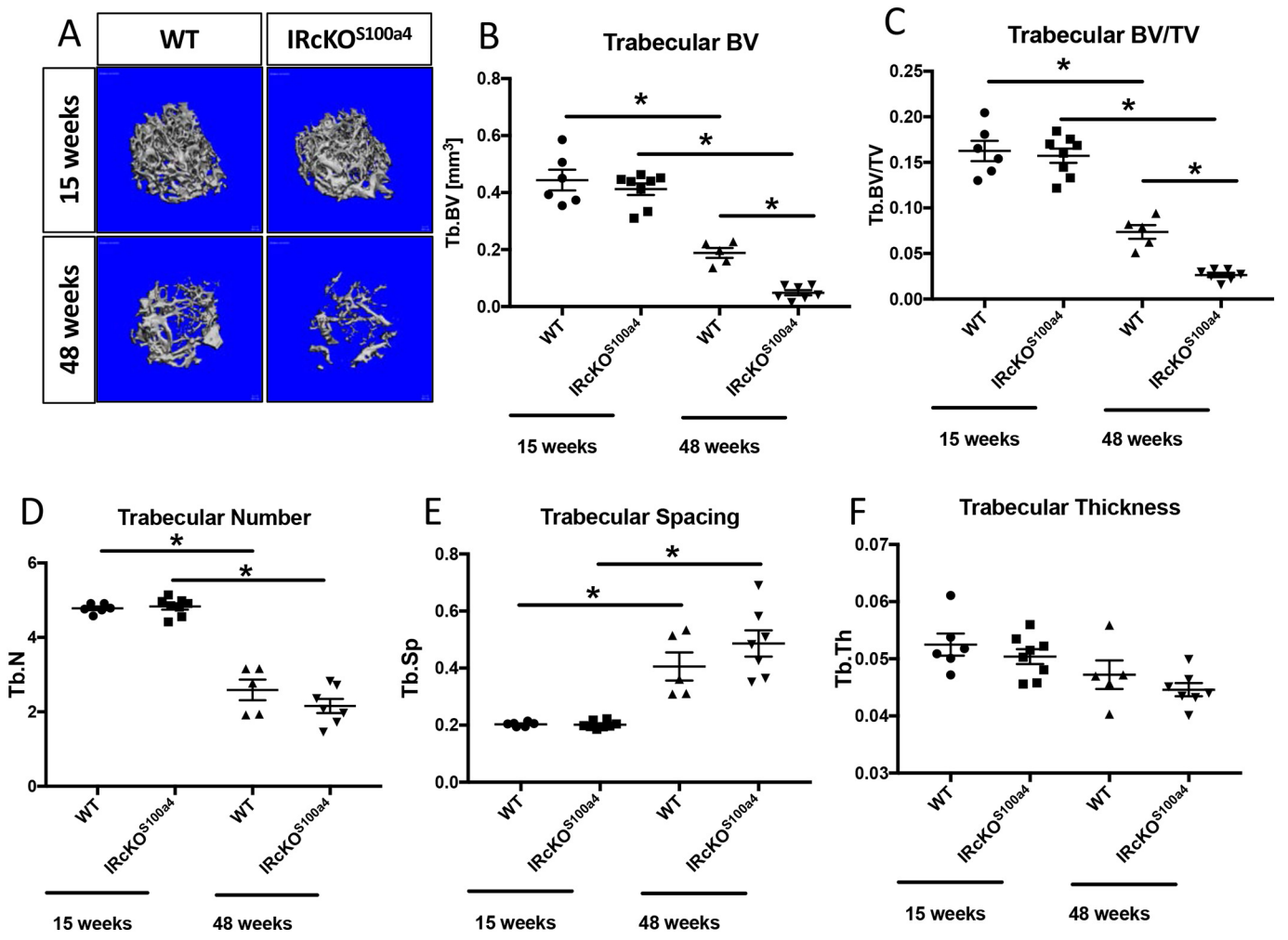

Fig. 5. IRcKO^{S100a4} enhances trabecular bone volume loss during aging. (A & B) 3D micro CT reconstructions of femur trabecular bone from (A) 15- and 48-week-old male mice. (B–F) Micro CT analysis of (B) Trabecular Bone Volume, (C) Trabecular Bone Volume/Total Volume, (D) Trabecular Number, (G) Trabecular Spacing, (F) Trabecular Thickness from WT and IRcKO^{S100a4} at 15 and 48 weeks of age. (*) indicates $p < 0.05$.

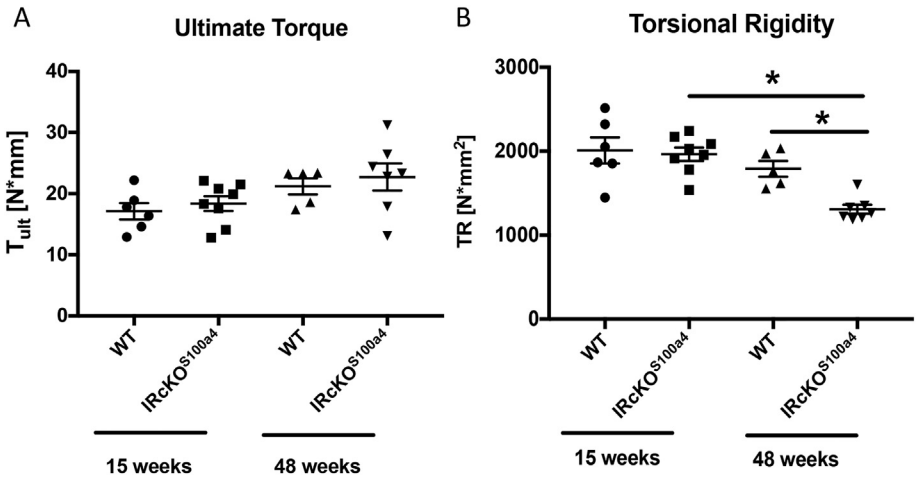

Fig. 6. IRcKO^{S100a4} decreases femur torsional rigidity at 48-weeks of age. To determine the effects of IRcKO^{S100a4} on the torsional mechanical properties, femurs from WT and IRcKO^{S100a4} littermates underwent torsion testing at 15- and 48-weeks of age to assess A) Ultimate Torque at Failure, and B) Torsional Rigidity. (*) indicates $p < 0.05$.

while there are more S100a4-lineage and actively expressing S100a4 cells during aging, the lack of cortical phenotype between WT and IRcKO^{S100a4} suggests that cortical bone maintenance is not regulated by IRβ in S100a4 cells. In contrast, dramatic trabecular bone phenotypes are observed between WT and IRcKO^{S100a4}, and many more trabecular bone cells retain S100a4 expression during aging, suggesting that IRβ expression in S100a4$^+$ cells is critical to trabecular bone homeostasis during aging. Finally, there are many S100a4-lineage cells are observed lining the endosteal surface, suggesting an additional cell population that may contribute to the observed phenotypes, although we have not specifically investigated this possibility.

In addition to assessing spatial localization of S100a4^{Ai9+} and

S100a4^{GFP+} cells, we have also assessed the relationship between S100a4-lineage cells and osteoblasts. Co-localization studies demonstrate that many S100a4-lineage cells also express markers of pre-osteoblasts (Osterix) and mature osteoblasts (Osteocalcin), suggesting that S100a4-lineage cells progress through osteoblast differentiation. Consistent with this, Duarte et al., observed that S100a4 was expressed by pre-osteoblasts, followed by a decline in expression in terminally differentiated osteocytes, in vitro (Duarte et al., 2003). These data suggest that IRcKO^{S100a4} results in deletion of IRβ in osteoblast precursors and a subset of mature osteoblasts, although the differences in phenotype compared to IR deletion in osteoblast lineages suggest that S100a4-cells may represent a potential discrete subpopulation of these cells. Consistent with this, we observed many Osteocalcin^{+} cells that are not derived from the S100a4-lineage, further supporting the differential phenotypes between IRcKO^{S100a4} and IRcKO^{Osteocalcin}.

There are several limitations to this study. First, the S100a4-Cre is non-inducible. Thus, we do not know the effects of delayed knock-down of IRβ in S100a4 cells. However, we have examined the bone phenotype in both young and aged mice, and do not observe any differences between genotypes in young mice. In addition, while S100a4-lineage cells are observed in trabecular bone and osteoblasts/osteocytes, and S100a4GFP^{Promoter} expression confirms active expression of S100a4 in these cells, it is not yet clear how S100a4 relates to other bone cell populations. Thus, future work will be needed to more clearly understand the lineage, fate and function of S100a4 cells in bone. Moreover, as we have not conducted histomorphometric analyses, it is unclear whether the bone phenotypes in IRcKO^{S100a4} are primarily driven by defects in osteoblast or osteoclast functions. Finally, we have only investigated the bone phenotypes in male mice, as these mice were obtained as part of separate study that focused on understanding diabetic tendinopathy (Studentsova et al., 2018). Since these mice were generated as a comparison to diet induced obesity/type II Diabetes in C57Bl/6J mice only male mice were used as female C57Bl/6J become obese but not diabetic (Surwit et al., 1988; Pettersson et al., 2012). Given the dramatic reduction in bone in female mice with aging, it will be important to understand how disruption of IRβ expression and signaling in S100a4-lineage cells may alter this phenotype in female mice. Finally, we only assessed the effects of IRcKO^{S100a4} on the femur, although other locations such as the Lumbar spine are also sensitive and susceptible to age-induced bone loss.

Taken together, these data demonstrate that deletion of IRβ in S100a4-lineage cells is sufficient to accelerate age-related trabecular bone loss and impair mechanics. This study defines the importance of determining how IR signaling in S100a4-lineage cells alters osteoblast, osteoclast and osteocyte function with the goal developing therapeutic approaches to prevent impaired IR signaling induced bone loss.

Author contributions

Study conception and design: AEL; Acquisition of data: VS, EK; Analysis and interpretation of data: VS, EK, AEL; Drafting of manuscript: AEL; Revision and approval of manuscript: VS, EK, AEL.

Transparency document

The Transparency document associated with this article can be found, in online version.

Acknowledgements

We would like to thank the Histology, Biochemistry and Molecular Imaging (HBMI) and the Biomechanics, Biomaterials and Multimodal Tissue Imaging (BBMTI) Cores for technical assistance. Research reported in this publication was supported by the National Institute of Arthritis and Musculoskeletal and Skin Diseases of the National Institutes of Health under Award Numbers K01AR068386, R01AR073169 and P30AR069655. The content is solely the responsibility of the authors and does not necessarily represent the official views of the National Institutes of Health.

References

Brown, M.L., Yukata, K., Farnsworth, C.W., Chen, D.G., Awad, H., Hilton, M.J., O'Keefe, R.J., Xing, L., Mooney, R.A., Zuscik, M.J., 2014. Delayed fracture healing and increased callus adiposity in a C57BL/6J murine model of obesity-associated type 2 diabetes mellitus. PLoS One 9 (6), e99656.

Bruning, J.C., Michael, M.D., Winnay, J.N., Hayashi, T., Horsch, D., Accili, D., Goodyear, L.J., Kahn, C.R., 1998. A muscle-specific insulin receptor knockout exhibits features of the metabolic syndrome of NIDDM without altering glucose tolerance. Mol. Cell 2 (5), 559–569.

Callis, G., Sterchi, D., 1998. Decalcification of bone: literature review and practical study of various decalcifying agents. Methods, and their effects on bone histology. J. Histotechnol. 21 (1).

Chau, D.L., Edelman, S.V., Chandran, M., 2003. Osteoporosis and diabetes. Curr. Diab. Rep. 3 (1), 37–42.

van Daele, P.L., Stolk, R.P., Burger, H., Algra, D., Grobbee, D.E., Hofman, A., Birkenhager, J.C., Pols, H.A., 1995. Bone density in non-insulin-dependent diabetes mellitus. The Rotterdam study. Ann. Intern. Med. 122 (6), 409–414.

Duarte, W.R., Shibata, T., Takenaga, K., Takahashi, E., Kubota, K., Ohya, K., Ishikawa, I., Yamauchi, M., Kasugai, S., 2003. S100A4: a novel negative regulator of mineralization and osteoblast differentiation. J. Bone Miner. Res. 18 (3), 493–501.

Erlandsson, M.C., Bian, L., Jonsson, I.M., Andersson, K.M., Bokarewa, M.I., 2013. Metastasin S100A4 is a mediator of sex hormone-dependent formation of the cortical bone. Mol. Endocrinol. 27 (8), 1311–1321.

Ferron, M., Wei, J., Yoshizawa, T., Del Fattore, A., DePinho, R.A., Teti, A., Ducy, P., Karsenty, G., 2010. Insulin signaling in osteoblasts integrates bone remodeling and energy metabolism. Cell 142 (2), 296–308.

Fulzele, K., Riddle, R.C., DiGirolamo, D.J., Cao, X., Wan, C., Chen, D., Faugere, M.C., Aja, S., Hussain, M.A., Bruning, J.C., Clemens, T.L., 2010. Insulin receptor signaling in osteoblasts regulates postnatal bone acquisition and body composition. Cell 142 (2), 309–319.

Gallant, M.A., Brown, D.M., Organ, J.M., Allen, M.R., Burr, D.B., 2013. Reference-point indentation correlates with bone toughness assessed using whole-bone traditional mechanical testing. Bone 53 (1), 301–305.

Gunczler, P., Lanes, R., Paz-Martinez, V., Martins, R., Esaa, S., Colmenares, V., Weisinger, J.R., 1998. Decreased lumbar spine bone mass and low bone turnover in children and adolescents with insulin dependent diabetes mellitus followed longitudinally. J. Pediatr. Endocrinol. Metab. 11 (3), 413–419.

Hadjidakis, D.J., Raptis, A.E., Sfakianakis, M., Mylonakis, A., Raptis, S.A., 2006. Bone mineral density of both genders in Type 1 diabetes according to bone composition. J. Diabetes Complicat. 20 (5), 302–307.

Inubushi, T., Lemire, I., Irie, F., Yamaguchi, Y., 2018. Palovarotene inhibits osteochondroma formation in a mouse model of multiple hereditary exostoses. J. Bone Miner. Res. 33 (4), 658–666.

Iwano, M., Plieth, D., Danoff, T.M., Xue, C., Okada, H., Neilson, E.G., 2002. Evidence that fibroblasts derive from epithelium during tissue fibrosis. J. Clin. Invest. 110 (3), 341–350.

Janghorbani, M., Feskanich, D., Willett, W.C., Hu, F., 2006. Prospective study of diabetes and risk of hip fracture: the Nurses' Health study. Diabetes Care 29 (7), 1573–1578.

Jiao, H., Xiao, E., Graves, D.T., 2015. Diabetes and its effect on bone and fracture healing. Curr. Osteoporos. Rep. 13 (5), 327–335.

Kayal, R.A., Tsatsas, D., Bauer, M.A., Allen, B., Al-Sebaei, M.O., Kakar, S., Leone, C.W., Morgan, E.F., Gerstenfeld, L.C., Einhorn, T.A., Graves, D.T., 2007. Diminished bone formation during diabetic fracture healing is related to the premature resorption of cartilage associated with increased osteoclast activity. J. Bone Miner. Res. 22 (4), 560–568.

Khan, T.S., Fraser, L.A., 2015. Type 1 diabetes and osteoporosis: from molecular pathways to bone phenotype. J. Osteoporos. 2015, 174186.

Kim, H., Lee, Y.D., Kim, M.K., Kwon, J.O., Song, M.K., Lee, Z.H., Kim, H.H., 2017. Extracellular S100A4 negatively regulates osteoblast function by activating the NF-kappaB pathway. BMB Rep. 50 (2), 97–102.

Kream, B.E., Smith, M.D., Canalis, E., Raisz, L.G., 1985. Characterization of the effect of insulin on collagen synthesis in fetal rat bone. Endocrinology 116 (1), 296–302.

Leclerc, E., Fritz, G., Vetter, S.W., Heizmann, C.W., 2009. Binding of S100 proteins to RAGE: an update. Biochim. Biophys. Acta 1793 (6), 993–1007.

Madisen, L., Zwingman, T.A., Sunkin, S.M., Oh, S.W., Zariwala, H.A., Gu, H., Ng, L.L., Palmiter, R.D., Hawrylycz, M.J., Jones, A.R., Lein, E.S., Zeng, H., 2010. A robust and high-throughput Cre reporting and characterization system for the whole mouse brain. Nat. Neurosci. 13 (1), 133–140.

Nicodemus, K.K., Folsom, A.R., Iowa, S., 2001. Women's health, type 1 and type 2 diabetes and incident hip fractures in postmenopausal women. Diabetes Care 24 (7), 1192–1197.

Pettersson, U.S., Walden, T.B., Carlsson, P.O., Jansson, L., Phillipson, M., 2012. Female mice are protected against high-fat diet induced metabolic syndrome and increase the regulatory T cell population in adipose tissue. PLoS One 7 (9), e46057.

Rakic, V., Davis, W.A., Chubb, S.A., Islam, F.M., Prince, R.L., Davis, T.M., 2006. Bone mineral density and its determinants in diabetes: the Fremantle Diabetes study. Diabetologia 49 (5), 863–871.

Randall, C., Mathews, P., Yurtsev, E., Sahar, N., Kohn, D., Hansma, P., 2009. The bone diagnostic instrument III: testing mouse femora. Rev. Sci. Instrum. 80 (6), 065108.

Rosen, D.M., Luben, R.A., 1983. Multiple hormonal mechanisms for the control of collagen synthesis in an osteoblast-like cell line, MMB-1. Endocrinology 112 (3), 992–999.
Saito, M., Marumo, K., 2013. Bone quality in diabetes. Front. Endocrinol. 4, 72.
Studentsova, V., Mora, K.M., Glasner, M.F., Buckley, M.R., Loiselle, A.E., 2018. Obesity/type II diabetes promotes function-limiting changes in murine tendons that are not reversed by restoring normal metabolic function. Sci. Rep. 8 (1), 9218.
Surwit, R.S., Kuhn, C.M., Cochrane, C., McCubbin, J.A., Feinglos, M.N., 1988. Diet-induced type II diabetes in C57BL/6J mice. Diabetes 37 (9), 1163–1167.
Thrailkill, K.M., Liu, L., Wahl, E.C., Bunn, R.C., Perrien, D.S., Cockrell, G.E., Skinner, R.A., Hogue, W.R., Carver, A.A., Fowlkes, J.L., Aronson, J., Lumpkin Jr., C.K., 2005. Bone formation is impaired in a model of type 1 diabetes. Diabetes 54 (10), 2875–2881.
Thrailkill, K., Bunn, R.C., Lumpkin Jr., C., Wahl, E., Cockrell, G., Morris, L., Kahn, C.R., Fowlkes, J., Nyman, J.S., 2014. Loss of insulin receptor in osteoprogenitor cells impairs structural strength of bone. J. Diabetes Res. 2014, 703589.
Vestergaard, P., 2007. Discrepancies in bone mineral density and fracture risk in patients with type 1 and type 2 diabetes—a meta-analysis. Osteoporos. Int. 18 (4), 427–444.